Some Analytic Integrals of the Averaged Variational Equations for a Thrusting Spacecraft

A. E. Petropoulos[1]

Starting with a numerical analysis of various thrust profiles for continuous-thrust escape from geostationary transfer orbit, we develop an averaging analysis that is valid for the full range of initial eccentricities (zero to almost one) and thrust-to-weight ratios. From the numerical analysis, it is found that shorter escape times are obtained when the phasing of the final revolution before escape yields an "escape from apoapsis" condition. This phasing is sensitive to slight variations in initial orbit and the exact thrust profile. In the averaging analysis, which bypasses this sensitivity, analytic integrals are found for the averaged variational equations for energy and eccentricity, based on elliptic integrals and series expansions thereof. Reasonably accurate explicit relations between mean energy and mean eccentricity, as well as time and these two quantities, are obtained for the full range of eccentricities and thrust ratios.

I. Introduction

The general problem of optimal continuous-thrust transfer between arbitrary orbits has not been solved analytically. Here we are particularly interested in the problem of low-thrust, spiraling escape or capture. Such spirals capitalize on the high specific impulse available to low-thrust engines, possibly reducing the required propulsion system and propellant mass. Over the last few decades, approximate solutions have been found for special cases. For example, as early as the late 1950s, Lawden [1,2] found that in the case of escape from a circular orbit using continuous, constant thrust acceleration, thrust in the tangential direction yields nearly the minimum characteristic velocity, the actual minimum occurring roughly for a thrust direction that bisects the tangential and circumferential directions. Indeed, several researchers [3–25] have obtained various approximate and sometimes exact analytic solutions for a number of specific initial orbits and specific thrust profiles, such as constant tangential thrust. Often, averaging methods are used either implicitly or explicitly. References [26–28] are excellent surveys of the older literature, capturing also the survey authors' insights.

Other research has focused directly on the problem of optimizing the spiraling trajectories, rather than identifying possible solutions only to the equations of motion. One of the earliest results was the analytic and now well-known Lawden's spiral [29,30]. A recently discovered analog has been obtained by Bishop and Azimov [31]. However, both of these apply only to highly specialized cases. Averaging

[1] Navigation and Mission Design Section.

The research described in this publication was carried out by the Jet Propulsion Laboratory, California Institute of Technology, under a contract with the National Aeronautics and Space Administration.

methods and the closely related method of multiple time scales [32] have been used in conjunction with the calculus of variations to provide both some analytic results for the case of low eccentricity and low thrust [33-35] and the basis for optimization software [36,37]. Direct methods, sometimes in conjunction with averaging, have also been used to avoid the complications of the large size of the multi-revolution spiraling problem [38,39]. Kechichian [40], rather than use averaging, adopts alternative coordinates that increase the speed of full, precise numerical integration, allowing the use of shooting methods to solve the two-point boundary-value problem (TPBVP) from the calculus of variations. The chosen coordinates also improve the convergence properties of the shooting method. To improve convergence in solving the TPBVP, other researchers [41,42] have found methods for obtaining better guesses for the initial values of the adjoint variables for circle-to-circle transfers. The recently developed static/dynamic control (SDC) algorithm [43,44], based in part on dynamic programming, has also been applied to the many-revolution, minimum-time escape problem [45], although its strengths currently lie in very high-fidelity, n-body optimization of trajectories with fewer than about a hundred revolutions.

We describe in this article the somewhat circuitous path which led to some analytic integrals of the averaged variational equations for a thrusting spacecraft. The integrals are valid for all initial eccentricities from slightly above zero to almost unity and for a wide range of initial thrust levels—in other words, over a large portion of the eccentricity-thrust space, with thrust measured relative to weight at a distance equal to the current semimajor axis. For the case of a continuously thrusting spacecraft, time is available analytically as a function of both average orbital energy and average eccentricity. Furthermore, analytic expressions for the time are obtained for the other regions of the eccentricity-thrust space, including the escape region, such that solutions may be patched together as the average osculating orbit moves between the regions. It should be noted that this approach is different from that of Shi and Eckstein [18], who use two-variable expansions that become decreasingly valid and increasingly unwieldy as the eccentricity and thrust increase.

The present integrals were found after investigating numerous empirically selected thrust profiles for the special case of escape from geostationary transfer orbit (GTO). First, we describe some of the thrust profiles, along with insights gained from the investigation. Using numerical integration of the equations of motion, we first determine the performance of tangential thrust over a wide range of initial eccentricities and periapse altitudes. Then, for the case of a nominal GTO initial orbit, we present four control laws for the thrust direction that out-perform the tangential-thrust law. The four laws have different functional forms which were selected from over fifteen functional forms that were studied in detail, each having its own set of parameters to adjust. The laws were selected based on their performance and on their perceived potential to serve in optimization as initial guesses that might not only speed up the optimization process, but also lead to different local minima. Second, we describe the integrals of the variational equations and the analytic relations for regions where the integrals are invalid.

II. Constant Tangential Thrust

We examine the time needed to escape from initial Earth orbits with a fixed periapsis altitude of 200 km and varying eccentricity. The following parameters are assumed: The thrust is constant at 465 mN, the specific impulse is 3100 s, the initial spacecraft mass is 1500 kg, the gravity field varies as $1/r^2$ with gravitational parameter 398,600.48504296 $\mathrm{km}^3/\mathrm{s}^2$, the Earth's radius is 6378.14 km, and thrust commences at periapsis. We define the nominal GTO to have a 200-km periapsis altitude and an apoapsis altitude of 35,786 km (eccentricity of about 0.730085). Shadowing and forces other than gravity are not considered.

For eccentricities near that of GTO, the escape time is found to oscillate significantly with initial eccentricity. This oscillation is depicted in Fig. 1. The equations of motion in polar coordinates are numerically integrated for various initial eccentricities while the initial periapsis altitude is fixed at 200 km. The oscillation occurs as an effect of phasing. The local minima in escape time are all seen to occur for

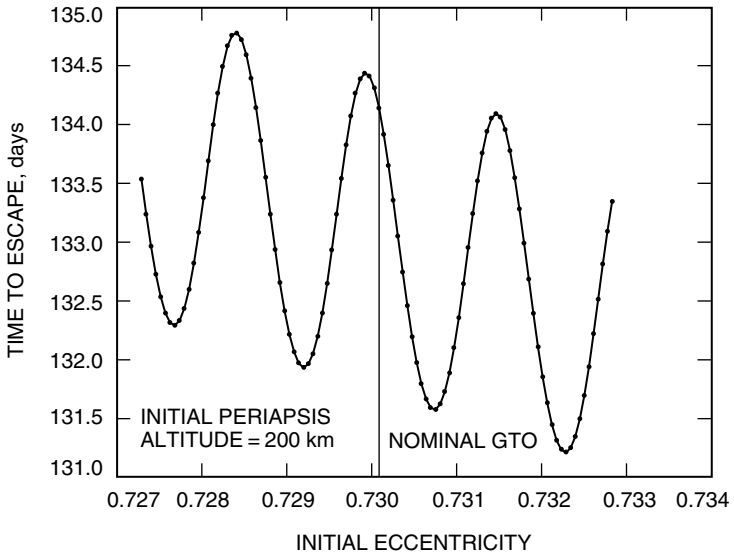

Fig. 1. Oscillation in escape time using tangential thrust for various initial Earth orbits near the nominal GTO, with thrust starting at periapsis.

those initial orbits where the osculating eccentricity of the spiral trajectory almost reaches zero shortly before escape, subsequently increasing roughly linearly with time to unity. In effect, "escape occurs from apoapsis," that is, at the point when the spacecraft has nearly reached the last apoapsis before escape, enough thrust is available to circularize the orbit, effectively turning apoapsis to periapsis and continuing with a positive and increasing flight-path angle up to escape. Whether the correct timing is obtained to effect these conditions depends on the initial orbit, since the thrust and gravitational parameters are assumed fixed. It is interesting to note in Fig. 1 that the difference between successive minima, about 0.36 days, is slightly less than the period of the nominal GTO, about 0.44 days, and that, while not evident in the figure, the successive minima differ by about one escape revolution (progressively fewer escape revolutions, the lower the local minimum).

Figure 2 shows as a function of initial eccentricity the minimum osculating eccentricity reached for each of the integrations performed in Fig. 1. The actual evolution of eccentricity with time is shown in Fig. 3 for two initial eccentricities: one giving the local maximum in escape time just prior to the nominal GTO line in Fig. 1 and one giving the local minimum just after the nominal GTO line. The oscillations in eccentricity with time have become almost diametrically out of phase well before the 80-day mark.

The local minima and maxima of escape time in Fig. 1 may be thought of as providing an envelope for the escape times. Figure 4 shows these envelopes for various initial periapsis altitudes and initial eccentricities varying from zero to about 0.85. As expected, the oscillations are of zero amplitude at zero eccentricity, and grow steadily with increasing eccentricity.

If we restrict ourselves to the nominal GTO initial orbit, we may instead adjust the thrust control law to obtain the correct phasing for escape from apoapsis. We now present four control laws that accomplish this.

III. Control Laws

In developing the control laws, two basic approaches are taken. The first is a simple trial-and-error approach, where the thrust angle is assumed to be of a certain functional form, with parameters in the functions serving as secondary controls that determine the precise thrust angle. The second approach,

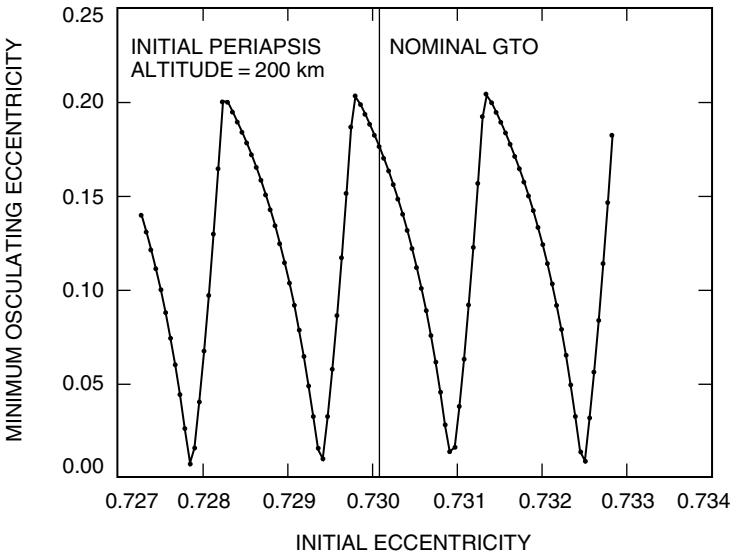

Fig. 2. Minimum osculating eccentricity reached using tangential thrust for various initial Earth orbits near the nominal GTO, corresponding to the cases in Fig. 1.

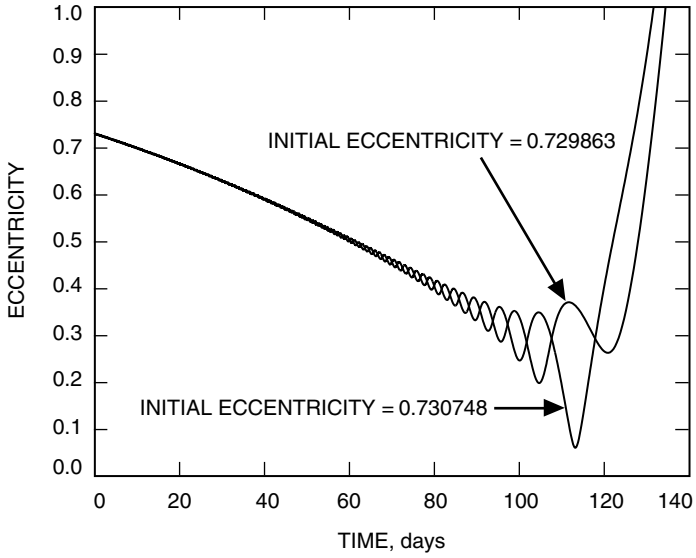

Fig. 3. Evolution of eccentricity with time for tangential thrust for orbits of the two different initial eccentricities that give the local maximum and minimum escape times immediately adjacent to the nominal GTO line in Fig. 1.

which might be termed a "guided trial-and-error approach," involves maximizing weighted averages of the rates of change of the osculating orbital elements. The exact weightings, or functional forms of the weightings, then become the secondary controls. This approach has been taken in the past, for example, by Kluever [46] and Gefert [47]. Thrust along the velocity vector, which maximizes the rate of increase of orbital energy (or, equivalently, semimajor axis), is the simplest example of this approach. For the numerical analysis of these control laws, apart from the thrust direction, all other parameters are taken to be the same as for the tangential-thrust case, and the initial orbit is taken as the nominal GTO.

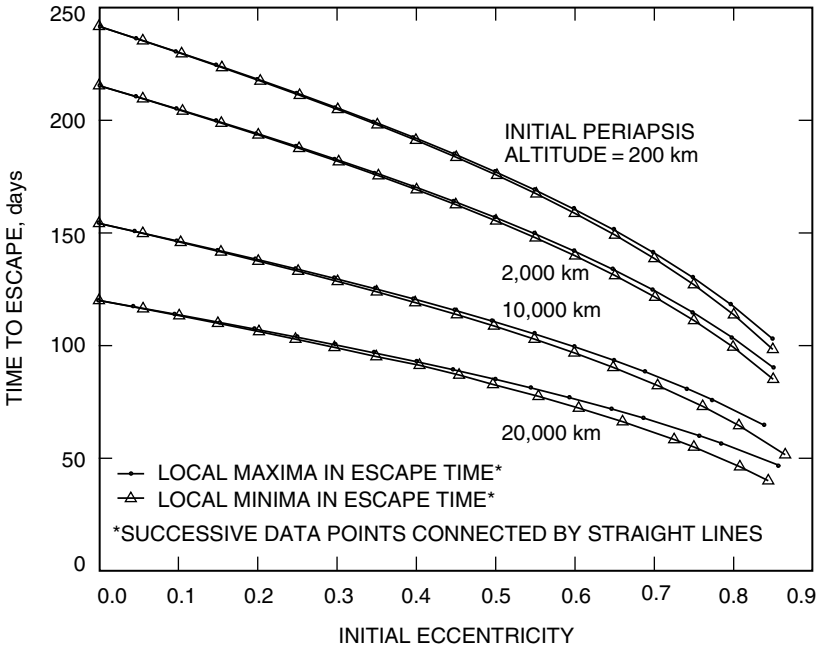

Fig. 4. Upper and lower bounds in escape time using tangential thrust for various initial Earth orbits, with thrust starting at periapsis.

The thrust direction is specified in terms of the thrust angle, α, which is measured from the circumferential direction, positive away from the gravitational center (as for the flight-path angle, γ). Three of the more successful trial-and-error functional forms for α, with numerical parameters tailored for low escape times from the nominal GTO, are given by

$$\alpha_{f11} = \gamma \left(1 + \mathrm{e}^{-n} - \mathrm{e}^{n(|\theta/\pi|-1)}\right)^{\mathrm{e}^{-[rv^2/(2\mu)]}}, \quad \text{with } n = 2 \tag{1}$$

$$\alpha_{f46} = \gamma - m|\sin\gamma|(\sin^2\gamma)^{\mathrm{e}^{n[rv^2/(2\mu)]}}, \quad \text{with } m = 33,\ n = 5 \tag{2}$$

$$\alpha_{f50} = \gamma_{(\theta+\phi)}, \quad \text{with } \phi = 8 \text{ deg} \tag{3}$$

where $\theta \in (-\pi, \pi]$ is the osculating true anomaly, r is the radius, v is the velocity, and μ is the gravitational parameter of the central body. It is evident that these three equations provide variations from the tangential-thrust law, $\alpha = \gamma$. In the last equation, for example, $\gamma_{(\theta+\phi)}$ represents a simple phase shift that gives the thrust angle as the flight-path angle not at the current position, but on the osculating conic at a true anomaly advanced by ϕ from the current osculating true anomaly.

An examination of the escape spiral for each of the control laws given by Eqs. (1) through (3) reveals that the escape from apoapsis characteristic is present in each case. With this observation in mind, we develop a thrust law based on maximizing the rate of decrease of the impulsive ΔV needed to escape from the osculating apoapsis radius. (In other words, the ΔV is that needed to escape, were the spacecraft to cease thrusting and perform an impulsive escape maneuver at the apoapsis of the osculating orbit.) The thrust angle giving the maximal rate of decrease is found using the variational equations for the semimajor axis, a, and the eccentricity, e, along with elementary conic relations. A weighting factor, c_w,

is included for added flexibility. The value $c_w = 1$ gives the maximal rate. An adjustment away from unity will typically be needed to give the minimum escape time. The thrust angle, then, is given by

$$\alpha_{f56} = \gamma - \frac{\pi}{2} - \text{atan}(c_w c_t, c_{no}) \tag{4}$$

where

$$c_t = \frac{av}{\sqrt{r_a \mu}} \left(\sqrt{1-e} - \sqrt{2} \right)$$

$$+ \frac{e + \cos\theta}{v} \sqrt{\frac{\mu}{r_a}} \left[\frac{2 - \sqrt{2(1-e)}}{(1+e)\sqrt{1-e}} \right] \tag{5}$$

$$c_{no} = \frac{r \sin\theta}{2av} \sqrt{\frac{\mu}{r_a}} \left[\frac{2 - \sqrt{2(1-e)}}{(1+e)\sqrt{1-e}} \right] \tag{6}$$

with r_a representing the osculating apoapsis radius, $r_a = a(1+e)$. The notation $\phi = \text{atan}(y, x)$ is shorthand for ($R \sin\phi = y$, $R \cos\phi = x$). For the nominal GTO, the weighting coefficient is set to $c_w = 2.8$ to obtain a favorable escape time.

For each law, the thrust angle and flight-path angle are depicted graphically in Fig. 5 as functions of the number of revolutions. The tangential-thrust law is designated α_{f1}. By looking at the flight-path angle, we see that the escape from apoapsis condition is present in the latter four control laws: The last local minimum in flight-path angle is very nearly zero and thereafter the flight-path angle rises increasingly fast with polar angle up to escape, that is, $\mathrm{d}^2\gamma/\mathrm{d}\theta^2$ is greater than zero, θ here being the polar angle. From the last local minimum, about half a revolution remains before escape.

The escape times and number of revolutions needed to escape are shown in Table 1 for each control law. It is noteworthy that the tangential-thrust law yields a longer escape time even though the number of full revolutions completed is one less than by the other control laws (93 full revolutions compared with 94). Recent work [45] has found that when used as initial guesses in optimization of the time to escape, the 94-revolution cases of Table 1 converge to a slightly higher local minimum when compared with the local minimum achieved from the tangential-thrust initial guess. (However, the optimization requires a longer computation time for the tangential-thrust case, as the initial guess for the escape time is further from the optimum than in the other cases.) The escape from apoapsis condition was found to be present in both local minima. The number of revolutions of the initial guess is retained in the optimal solution, suggesting that initial guesses requiring fewer revolutions to escape be preferred in optimization, even if their escape time is longer. Interestingly, an examination of all the control-law functional forms that were studied, of which tangential thrust and Eqs. (1) through (4) are a subset, reveals that those with fewer full escape revolutions typically had longer escape times.

Given the laborious nature of numerical integration and the tuning of a particular control law for a particular initial orbit, we turn now to an averaging analysis to obtain estimates of escape times and other characteristics of the escape spiral without the need of either selecting or numerically integrating an exact thrust profile. In addition to the analytical insights and computational simplifications to be gained, the sensitivity of the escape time not only to the initial orbit, but also to the control law and the parameters that govern it, will be reduced.

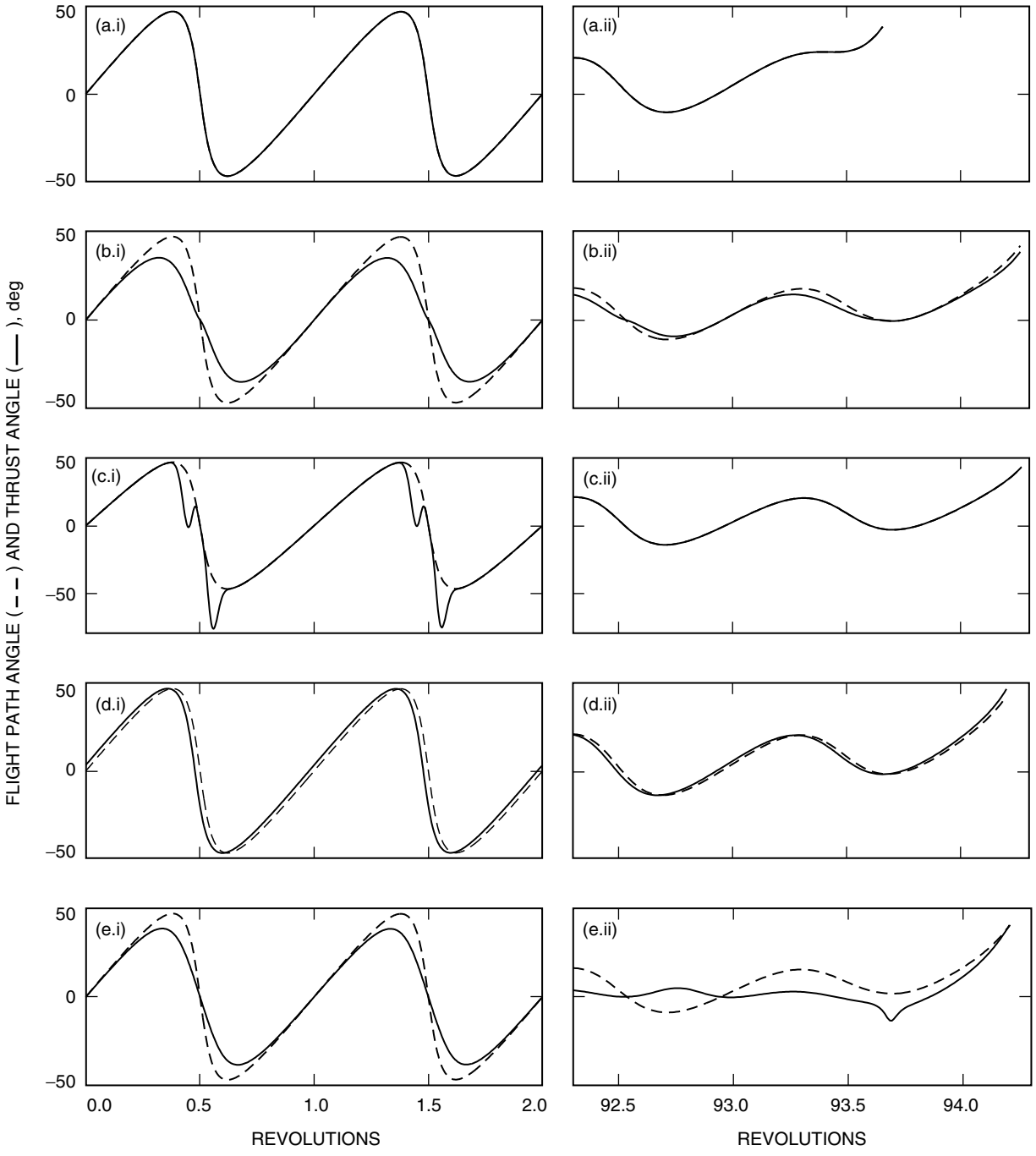

Fig. 5. Thrust angles and flight-path angles of five different control laws for escape from GTO: (a) α_{f1}, tangential thrust, (b) α_{f11} control law, (c) α_{f46} control law, (d) α_{f50} control law, and (e) α_{f56} control law. Shown for the first few revolutions (i) and the last few revolutions (ii).

Table 1. Comparison of times and revolutions to escape from the nominal GTO, using different control laws.

Control law	Escape time, days	Escape revolutions
α_{f1}	134.14	93.7
α_{f11}	131.76	94.3
α_{f46}	132.00	94.3
α_{f50}	132.20	94.2
α_{f56}	132.19	94.2

IV. Averaging Analysis

As before, we restrict ourselves here to thrusting that remains in the orbital plane. We develop an analysis based on solving the averaged variational equations using elliptic integrals and series expansions thereof. Perhaps the simplest starting point is an inspection of the behavior of the specific orbital energy, $\mathcal{E}$,

$$\mathcal{E} = -\frac{\mu}{2a} \tag{7}$$

where μ is the gravitational parameter of the central body and a is the semimajor axis, as before. From elementary orbital mechanics, we see that the energy is changed only by that component of thrust acting tangentially to the orbit:

$$\mathrm{d}\mathcal{E} = f_t \mathrm{d}s \tag{8}$$

where f_t is the component of thrust acceleration acting along the velocity vector and s is the path length. Of course, this reduces immediately to the customary variational equation for semimajor axis (see, for example, Battin [48, p. 489]):

$$\frac{\mathrm{d}a}{\mathrm{d}t} = \frac{2a^2 v}{\mu} f_t \tag{9}$$

However, it is more illuminating to remain with the formulation in terms of path length, for it affords geometrical insights. We know that when the thrust is small, the orbit will not change size or shape significantly over the course of one revolution. Thus, we may approximate the path length traversed by the spacecraft over one full revolution as the perimeter of the initial ellipse, S_p:

$$S_p = 4aE_I(e) \tag{10}$$

where

$$E_I(e) = \int_0^{\pi/2} \sqrt{1 - e^2 \sin^2\theta}\, \mathrm{d}\theta \tag{11}$$

is the complete elliptic integral of the second kind with modulus equal to the eccentricity, e. (We use E_I instead of the customary symbol, E, to avoid confusion with the established notation for the eccentric anomaly, to be used later.) Then, assuming that f_t does not change very much, the change in energy over one full revolution is approximately

$$\Delta\mathcal{E}^{2\pi} \approx 4 f_t a E_I(e) \tag{12}$$

The time-averaged rate of change of energy over one revolution is then simply obtained by dividing the change in energy by the period of the initial orbit,

$$\overline{\frac{\mathrm{d}\mathcal{E}}{\mathrm{d}t}}^{t,2\pi} \approx \frac{2 f_t}{\pi}\sqrt{\frac{\mu}{a}} E_I(e) \tag{13}$$

For the circular orbit, this reduces to the well-known $f_t\sqrt{\mu/a}$, since $E_I(0) = \pi/2$.

On the right-hand side of Eq. (13) there appear the orbital parameters a and e, the former a known function of $\mathcal{E}$ but the latter of as yet undetermined functional dependence on $\mathcal{E}$ or t. Thus, we turn now to the variational equations for eccentricity, and osculating eccentric anomaly, E (see, for example, Battin [48, p. 489]):

$$\frac{\mathrm{d}e}{\mathrm{d}t} = \frac{1}{v}\left[2\left(e + \cos\theta\right) f_t + \frac{r}{a} f_n \sin\theta\right] \tag{14}$$

$$\frac{\mathrm{d}E}{\mathrm{d}t} = \frac{na}{r} - \frac{1}{ebv}\left[2a f_t \sin\theta - r\left(e + \cos\theta\right) f_n\right] \tag{15}$$

where v is the velocity, θ is the osculating true anomaly, r is the radius, f_n is the component of thrust acceleration normal to the velocity vector and away from the gravitating center (cf., Battin [48], who uses the inward normal direction instead), $n = \sqrt{\mu/a^3}$ is the mean motion, and $b = a\sqrt{1-e^2}$ is the semiminor axis. Equation (15) may be approximated as

$$\frac{\mathrm{d}E}{\mathrm{d}t} \approx \frac{na}{r} \tag{16}$$

when the eccentricity is greater than some small positive value, and when the thrust acceleration is small compared to the gravitational acceleration. What "small" means will be investigated later, as will the behavior when these criteria are not satisfied. We may then approximate the rate of change of eccentricity with eccentric anomaly as

$$\frac{\mathrm{d}e}{\mathrm{d}E} \approx \frac{r}{na}\frac{\mathrm{d}e}{\mathrm{d}t} \tag{17}$$

Using Eq. (14) and various relations for conic sections, the right-hand side of Eq. (17) may be written in terms of a, e, E, f_t, and f_n. If we assume that all of these except E do not change significantly over the course of one revolution, we may treat them as constant. With this approximation, after numerous algebraic manipulations and changes of variables, we are able to find an integral of the right-hand side for any initial and final values of E. For one full revolution in E (approximately one full revolution in polar angle), the integral reduces to

$$\overline{\Delta e}^{2\pi} \approx -\frac{8 f_t (1-e^2)}{e\mu/a^2}\big[K(e) - E_I(e)\big] \tag{18}$$

where

$$K(e) = \int_0^{\pi/2} \frac{\mathrm{d}\theta}{\sqrt{1 - e^2 \sin^2\theta}} \tag{19}$$

is the complete elliptic integral of the first kind with modulus equal to the eccentricity, e. Notably, over one full revolution, the normal thrust has no effect. As with the energy, we may compute the time-averaged rate of change of eccentricity over one revolution:

$$\overline{\frac{\mathrm{d}e}{\mathrm{d}t}}^{t,2\pi} \approx -\frac{4 f_t (1-e^2)}{\pi e}\sqrt{\frac{\mu}{a}}\big[K(e) - E_I(e)\big] \tag{20}$$

An averaged differential relation solely between energy and eccentricity is now forthcoming from Eqs. (12) and (18):

$$\overline{\frac{\mathrm{d}\mathcal{E}}{\mathrm{d}e}}^{t,2\pi} = \frac{\overline{\Delta\mathcal{E}}^{2\pi}}{\overline{\Delta e}^{2\pi}} \approx -\frac{\mu}{2a} \cdot \frac{e E_I(e)}{(1-e^2)\big[K(e) - E_I(e)\big]} \tag{21}$$

We henceforth discontinue the cumbersome overbar notation for averaged quantities. It should be clear from the context when time-averaged quantities are being used. It should also be noted that the relationship between the e and $\mathcal{E}$ of the starting orbit and their respective averaged values over the next revolution depends on where on the orbit the thrust commences. For simplicity, we assume the thrust to commence at periapsis, since then the initial values for e and $\mathcal{E}$ are close to the average values over the next revolution. After another series of manipulations, using relations between elliptic integrals listed in Gradshteyn and Ryzhik [49], Eq. (21) may be integrated to yield

$$\frac{\mathcal{E}}{\mathcal{E}_0} \approx \frac{\big[K(e) - E_I(e)\big]}{\big[K(e_0) - E_I(e_0)\big]} \tag{22}$$

where the subscript 0 denotes values on the initial orbit. Remarkably, the thrust acceleration components, as long as they remain roughly constant, do not affect the relation between energy and eccentricity.

In order to find the dependence of the energy and eccentricity on time, we return to Eq. (13), which we integrate with the help of Eq. (22), integration variable changes, and series expansions in selected variables involving elliptic integrals (partly from Gradshteyn and Ryzhik [49]). For greater generality, we introduce as a time-like variable the characteristic velocity of the thrusting spiral:

$$\Delta V = \int_0^t f_t \mathrm{d}t \tag{23}$$

In the simplest case, f_t is constant, and $t = \Delta V / f_t$. Another common case is that of constant thrust and constant specific impulse, where the time is related to the ΔV by

$$t = \frac{c}{f_{t0}} \left(1 - \mathrm{e}^{-[\Delta V/c]}\right) \tag{24}$$

with c denoting the exhaust velocity and f_{t0} the initial thrust acceleration. Thus, the integration of Eq. (13) yields

$$\begin{aligned}\Delta V \approx \pi\sqrt{\frac{-\mathcal{E}_{e0}}{2}} \Bigg\{ & \frac{2}{\pi}\left[\left(\frac{\mathcal{E}_0}{\mathcal{E}_{e0}}\right)^{1/2} - \left(\frac{\mathcal{E}}{\mathcal{E}_{e0}}\right)^{1/2}\right] + \frac{2}{3\pi^2}\left[\left(\frac{\mathcal{E}_0}{\mathcal{E}_{e0}}\right)^{3/2} - \left(\frac{\mathcal{E}}{\mathcal{E}_{e0}}\right)^{3/2}\right] \\ & + \frac{1}{10\pi^3}\left[\left(\frac{\mathcal{E}_0}{\mathcal{E}_{e0}}\right)^{5/2} - \left(\frac{\mathcal{E}}{\mathcal{E}_{e0}}\right)^{5/2}\right] - \frac{3}{14\pi^4}\left[\left(\frac{\mathcal{E}_0}{\mathcal{E}_{e0}}\right)^{7/2} - \left(\frac{\mathcal{E}}{\mathcal{E}_{e0}}\right)^{7/2}\right] \\ & - \frac{107}{288\pi^5}\left[\left(\frac{\mathcal{E}_0}{\mathcal{E}_{e0}}\right)^{9/2} - \left(\frac{\mathcal{E}}{\mathcal{E}_{e0}}\right)^{9/2}\right]\Bigg\}\end{aligned} \tag{25}$$

and

$$\begin{aligned}\Delta V \approx \sqrt{\frac{-\mathcal{E}_{e0}\pi}{2}} \Bigg[& (e_0 - e) + \frac{13}{48}\left(e_0^3 - e^3\right) + \frac{383}{2,560}\left(e_0^5 - e^5\right) \\ & + \frac{5,833}{57,344}\left(e_0^7 - e^7\right) + \frac{43,649}{589,824}\left(e_0^9 - e^9\right)\Bigg]\end{aligned} \tag{26}$$

where

$$\mathcal{E}_{e0} = \frac{\mathcal{E}_0}{\left[K(e_0) - E_I(e_0)\right]} \tag{27}$$

Either of Eqs. (25) and (26) may be used to obtain the ΔV (and hence the time), although their results will be slightly different due to different truncation errors in the series.

We examine now the region of validity of the assumption that the thrust is small, which allowed us to make the approximation of Eq. (16). First we note from Eq. (22) that, as energy increases, the eccentricity decreases. However, we know that when the energy reaches zero, the eccentricity must be unity, because the radial distance of the spacecraft is finite due to the finite time needed to escape. Thus, at some point the eccentricity must cease to decrease and instead increase. We know from the preceding sections, which studied escape from GTO, that the escape from apoapsis characteristic, typically present in escape spirals with favorable escape times, involves near-circularization about one half revolution in polar angle before escape. Up to this circularization, a revolution in polar angle corresponds roughly to a revolution in osculating eccentric anomaly. Thus, just prior to circularization, we estimate the change in energy per polar angle revolution to be equal to the change in energy over one E-revolution. It is convenient to introduce the parameter q as the number of quarter revolutions in polar angle that remain until escape. At circularization, q will be about 2, and we may approximate the change in energy over the next q quarter revolutions in E, $q\overline{\Delta\mathcal{E}}^{\pi/2}$, as the energy needed to escape. Using Eqs. (12) and (22) along with judicious series expansions, we may determine the mean eccentricity at which q quarter revolutions remain until escape:

$$e_{xen}^2 = \frac{8}{3\left(1+\dfrac{4\pi\mu/a_0^2}{3qf_t[K(e_0)-E_I(e_0)]^2}\right)}\left(\sqrt{4+\frac{4\pi\mu/a_0^2}{qf_t\left[K(e_0)-E_I(e_0)\right]^2}}-1\right) \tag{28}$$

The subscript *xen* denotes energy-based cut-off. Once the mean eccentricity reaches e_{xen}, energy is approximated as increasing linearly with time up to escape. As a cruder approximation, we also take eccentricity to increase linearly with time up to unity. Since we know both the time of the cut-off [from Eq. (26)] and the rate of change of energy [from Eq. (13)], we can easily estimate the time to escape.

We now turn to the requirement, for the approximation Eq. (16) to be valid, that eccentricity be greater than some small number. As the mean eccentricity decreases with increasing energy, there may come a time when the oscillations about the mean are large enough that the osculating eccentricity will reach zero. To estimate the amplitude of the oscillations, we approximate the osculating eccentricity as a sinusoidal variation with E, superimposed on the negligibly varying mean eccentricity, with different amplitude on the outbound part of the spiral than on the inbound. We also assume f_n to be zero, although a corresponding analysis with non-zero f_n should yield similar results, but more laboriously. Accounting for the difference in $\dot{E}$ between periapsis and apoapsis, we find the minimum osculating eccentricity over the course of one revolution approximately as

$$e_{\min} \approx e - \frac{2f_t}{\mu/a^2}(1+e)\sqrt{1-e^2} \tag{29}$$

where e and a are mean values. The minimum permissible value, e_{x0}, of the mean eccentricity is thus that value which makes $e_{\min}$ zero. Rearranging Eq. (29), we obtain a quartic in e_{x0}:

$$e_{x0}^4 - 2e_{x0}^3 + \left(\frac{\mu/a^2}{2f_t}\right)^2 e_{x0}^2 - 2e_{x0} - 1 \approx 0 \tag{30}$$

We may ignore third- and higher-order terms in e_{x0} to obtain

$$e_{x0} \approx \left(\frac{2f_t}{\mu/a^2}\right)\sqrt{1+\left(\frac{2f_t}{\mu/a^2}\right)^2} + \left(\frac{2f_t}{\mu/a^2}\right)^2 \tag{31}$$

This is an excellent approximation, even as escape is approached, because the coefficient of e_{x0}^2 in Eq. (30) is the dominant one very nearly up to escape. When $2f_t/(\mu/a^2)$ is small, Eq. (31) can be further simplified to the very compact

$$e_{x0} \approx \frac{2f_t}{\mu/a^2} \tag{32}$$

Another possible approximation is to ignore terms of order two and higher in e in Eq. (29), which results in

$$e_{x0} \approx \frac{\dfrac{2f_t}{\mu/a^2}}{1-\dfrac{2f_t}{\mu/a^2}} \tag{33}$$

The quantity e_{x0} of Eqs. (30) through (33) may be interpreted as the mean eccentricity of an escape spiral that commences from an initially circular orbit, or, in fact, any orbit with eccentricity less than e_{x0}, for the mean eccentricity cannot be less than this value because $e_{\min}$ would be less than zero, and, should it rise above e_{x0}, it would quickly descend again, based on Eq. (22). Near escape we may obtain an analogous relation to Eq. (28): We estimate that when q quarter revolutions remain to escape, the energy continues to change at the same rate up to escape. With Eqs. (12) and (33) and the appropriate series expansions, the mean eccentricity at which q quarter revolutions remain to escape is found to be

$$e_{xen0} \approx \frac{1}{\frac{\pi}{2}q - 1} \tag{34}$$

When about one revolution remains to escape ($q \approx 4$), an examination of Eqs. (31) and (34) shows that the mean eccentricity is just beginning to rise very quickly with $2f_t/(\mu/a^2)$. As Eq. (34) thus becomes increasingly inaccurate, we instead estimate that the energy and eccentricity increase linearly with time after the eccentricity has reached e_{xen0} with $q \approx 4$. In the region where the mean eccentricity of the escape spiral remains below e_{xen0}, rather than use Eq. (32) to integrate Eq. (13), we just rearrange Eq. (32) using our observation that e_{x0} is also the mean eccentricity for near-circular spirals. The rearrangement provides, for the case of constant f_t, the evolution of mean eccentricity and mean energy from their initial values:

$$\frac{e}{e_0} \approx \frac{\mathcal{E}_0^2}{\mathcal{E}^2} = \frac{v_{c0}^4}{v_c^4} \tag{35}$$

where $v_c = \sqrt{\mu/a}$ is the circular orbit speed. This expression may still be used with some accuracy when f_t is only nearly constant. The characteristic velocity, and hence the time, may be found by substituting Eq. (35) into Eq. (13) and integrating with suitable changes in integration variable and series expansions. The ΔV may be expressed both in terms of the mean circular orbit speed and the mean eccentricity:

$$\begin{aligned}\Delta V \approx v_{c0} \Bigg\{ &\left(1 - \frac{v_c}{v_{c0}}\right) + \frac{e_0^2}{28}\left[\left(\frac{v_{c0}}{v_c}\right)^7 - 1\right] + \frac{7e_0^4}{960}\left[\left(\frac{v_{c0}}{v_c}\right)^{15} - 1\right] \\ &+ \frac{15e_0^6}{5,888}\left[\left(\frac{v_{c0}}{v_c}\right)^{23} - 1\right] + \frac{723e_0^8}{507,904}\left[\left(\frac{v_{c0}}{v_c}\right)^{31} - 1\right]\Bigg\} \end{aligned} \tag{36}$$

$$\begin{aligned}\approx v_{c0} \Bigg\{ &\left[1 - \left(\frac{e_0}{e}\right)^{1/4}\right] + \frac{1}{28}\left[e^2\left(\frac{e_0}{e}\right)^{1/4} - e_0^2\right] + \frac{7}{960}\left[e^4\left(\frac{e_0}{e}\right)^{1/4} - e_0^4\right] \\ &+ \frac{15}{5,888}\left[e^6\left(\frac{e_0}{e}\right)^{1/4} - e_0^6\right] + \frac{723}{507,904}\left[e^8\left(\frac{e_0}{e}\right)^{1/4} - e_0^8\right]\Bigg\} \end{aligned} \tag{37}$$

Recall that e_0 is not the initial orbit eccentricity, but the initial mean eccentricity to be determined from any of Eqs. (30) through (33).

Lastly, we determine the point where the mean eccentricity falls below the minimum permissible value, e_{x0}, for an escape spiral with initially decreasing mean eccentricity. Equation (33) is sufficiently accurate and also sufficiently simple to allow simultaneous solution with Eq. (22), with the aid of series expansions

for the elliptic integrals, as usual. The eccentricity that satisfies both equations is, to first order in eccentricity,

$$e_{xce} \approx \frac{5c_e}{5 - c_e} \tag{38}$$

and, to second order in eccentricity,

$$e_{xce} \approx \frac{5(5 - c_e)}{4c_e} \left[\sqrt{1 + 8 \left(\frac{c_e}{5 - c_e} \right)^2} - 1 \right] \tag{39}$$

where

$$c_e = \left\{ \frac{32 f_{tx}}{\pi^2 \mu / a_0^2} \left[K(e_0) - E_I(e_0) \right] \right\}^{1/5} \tag{40}$$

In the latter expression, f_{tx} is the tangential thrust acceleration at the time when the two curves [Eqs. (22) and (33)] intersect. If f_t is not constant, typically only a small correction will be needed. For example, with constant thrust, constant, high specific impulse, and large initial mass, the thrust acceleration normally will increase only slightly, an effect that can be accounted for by solving Eq. (38) [or Eq. (39)] iteratively with Eqs. (26) and (24). (One iteration normally will be sufficiently accurate. Analytic approximations may also be available.)

The above observations may be summarized on a plot of eccentricity versus "thrust to semimajor weight" ratio, $f_t/(\mu/a^2)$, where different regions may be identified based on which of the preceding analyses are applicable. For ease of reference to this type of plot, we use the term "ef-plot." For simplicity, we describe spirals of increasing energy, although a parallel development is possible for spirals of decreasing energy. In Fig. 6, the circularization boundary, C_B, provides not only the mean eccentricity for initial orbits with eccentricity and thrust to semimajor weight on or below the boundary, but also the lower bound in mean eccentricity for spirals starting above the boundary. It is obtained from Eq. (33). Below the circularization boundary is the circular region, C, which is bounded on the right by the Q_{q_c} line (Q_4 line in Fig. 6), that is, the line where q_c quarter revolutions remain to escape—the value of q_c being taken as 4, in accordance with the discussion of Eq. (34), which provides the intersection point of the C_B curve and the Q_{q_c} line. In Fig. 6, the Q_{q_c} line is labeled Q_4, and the intersection with C_B is labeled C_4.

Regions S and E in Fig. 6 are both "elliptic" regions. In particular, Eqs. (12) through (27) (what might be termed the elliptic analysis) are applicable to spirals starting in these regions. Region E is the pure elliptic region, so named because spirals starting in this region remain within the elliptic region until they reach the Q_{q_e} line, on which q_e quarter revolutions remain to escape. According to the discussion of Eq. (28), q_e is taken as 2 in the figure, and so the line is labeled Q_2. Region S, on the other hand, is named the semi-elliptic region because spirals starting therein will meet the circularization boundary, C_B, at a point below C_4. Thereafter, the spirals follow the circular analysis up to C_4. The boundary between the S and E regions is named the semi-elliptic boundary, S_B. It is computed using Eq. (22) with constant f_t and the eccentricity at the C_4 point. Its intersection with the Q_2 line, labeled S_2, is obtained from Eq. (28). For near-constant f_t, as in the constant-thrust, constant-I_{sp} case, the precise boundary between the S and E regions is close to S_B. Rather than compute the precise boundary, following the discussion of Eqs. (38) and (39), one can assess whether a chosen starting point in the elliptic region will intersect the circularization boundary at eccentricities below the C_4 point, or whether it will continue to the Q_2 boundary.

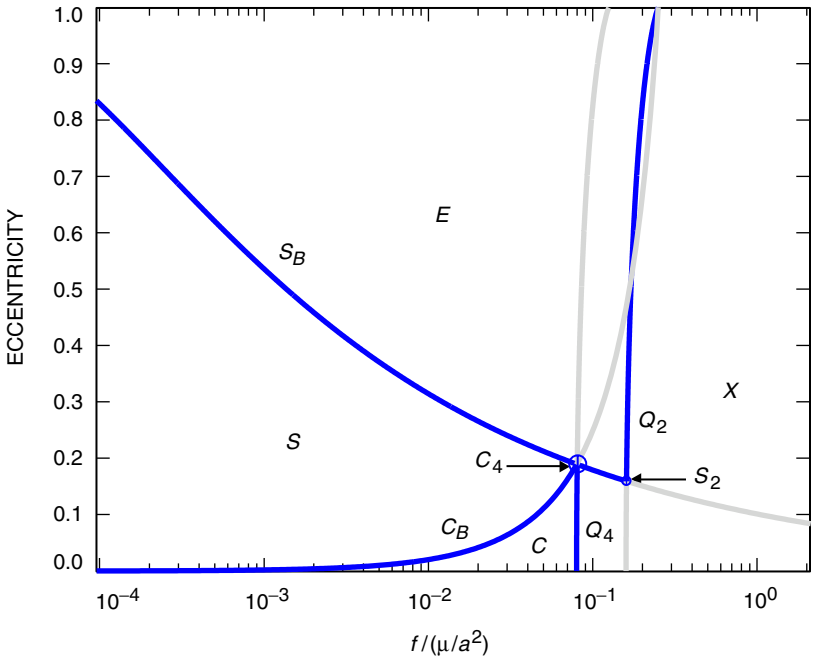

Fig. 6. Regions of the ef-plot (eccentricity versus thrust-to-semimajor-weight ratio): circular region, *C*; semi-elliptic region, *S*; pure elliptic region, *E*; escape region, *X*; circularization boundary, C_B; semi-elliptic boundary, S_B; four and two quarter revolutions to escape curves, Q_4, Q_2; terminus of C_B on Q_4, C_4; and terminus of S_B on Q_2, S_2. The light gray parts of curves are not active boundaries.

Region X in Fig. 6 is the escape region. It is bounded on the left by the Q_2 line, the part of S_B between C_4 and S_2, and the Q_4 line. The simple approximation that the rate of change of mean energy remains constant from this left-hand boundary up to escape is quite accurate. Matching of the second derivative of energy could provide even greater accuracy, should it be desired. The eccentricity may be roughly modeled as increasing linearly with time from this boundary up to escape. Starting within the X region, one can use Eq. (13) for the rate of change of energy.

The C_B, S_B, Q_4, and Q_2 curves in Fig. 6 are drawn in light-grey where they do not serve as demarcators of regions. We recall, however, that the active parts of these curves depend on the choice of q_c and q_e, which have been taken as 4 and 2, respectively, in the figure. Of course, the intersection points of the curves could be calculated for other values.

V. Comparisons of Averaging with Full Numerical Integration

As a first example, we return to our original problem of escape from GTO, to determine the efficacy with which the averaging analysis predicts the time of flight to escape. The numerical analysis in this section uses the same parameters as in the constant tangential-thrust section. The dependence of the tangential-thrust escape time on the exact initial orbit was shown already in Fig. 1. All of the orbits of the figure fall in region E of Fig. 6. Applying the elliptic analysis to them, with $q_e = 2$ and with $q_e = 3$, we find the escape times shown in Fig. 7, which includes the original data of Fig. 1 for easy comparison. We see that the averaging analysis with $q_e = 2$ provides a good estimate of the moving average escape time, while the $q_e = 3$ curve provides an optimistic estimate of the minimum escape time. The escape time for the α_{f11} control law applied to the nominal GTO is seen to be just above the line joining the

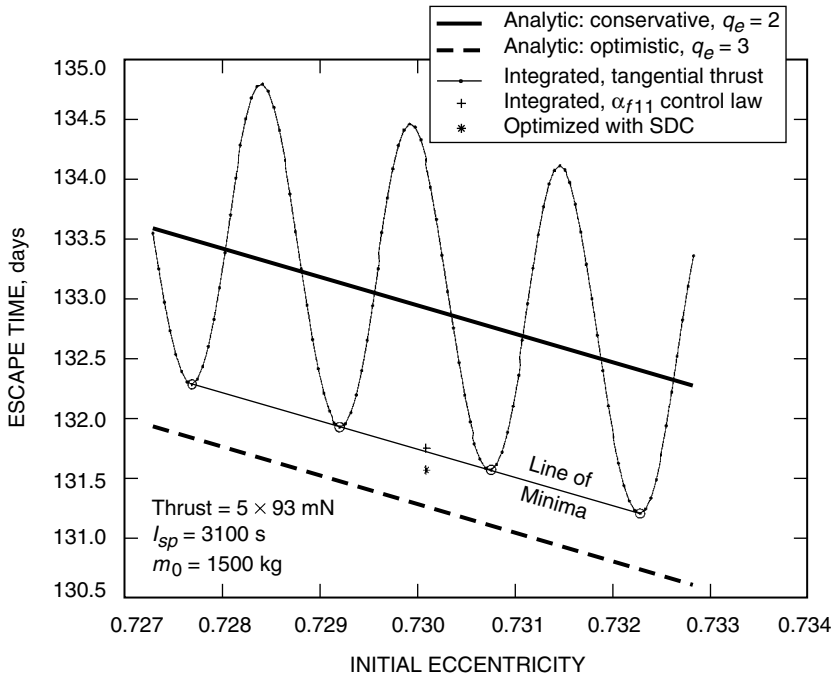

Fig. 7. Comparison of escape times computed by numerical integration and by the averaging analysis for orbits near GTO.

minima in escape time for the tangential-thrust case. The escape time from GTO, as optimized[2] using SDC [43,44], is also shown in the figure for comparison.

We now extend the escape time comparison to the same wide range of initial orbits of Fig. 4. The data of that figure are reproduced in Fig. 8 alongside data obtained from the averaging analysis. The standard values of $q_e = 2$ and $q_c = 4$ are used. The parameter $t_{ecut} = 1$ specifies that the time at C_4 or S_2 is computed using Eq. (37) or Eq. (26), respectively. With $t_{ecut} = 2$, the times are instead computed using Eq. (36) or Eq. (25), respectively. (In Fig. 7, the value $t_{ecut} = 2$ was used.) The small discontinuities in the curves for the averaging analysis are due to initial orbits lying in different regions of the ef-plot. The zoomed subplots show more clearly all the discontinuities due to initial orbits switching from the S region to the E region. The escape time from the averaging analysis is seen to be close to the numerical integration values. The fact that the times match better for initial orbits in the E region perhaps belies the greater accuracy of the analysis in that region compared to the analysis for the circularization boundary, along which spirals starting in the S region must eventually travel.

Figure 9 shows the demarcations of the regions of the ef-plot (Fig. 6) together with traces of spirals computed using numerical integration for various starting conditions, labeled A through F. The dashed lines indicate the corresponding behavior predicted by the averaging analysis for starting conditions C through F which lie in the elliptic regions (S and E). That is, the dashed lines, which might be termed elliptic averaging contours, are valid only up to their intersection with the circularization boundary (C_B) or the Q_2 line. The elliptic averaging contours for C and D intersect C_B, whereupon the numerically integrated solution begins to oscillate roughly about C_B instead of about the elliptic averaging contour. The C_B curve is roughly followed up to the Q_4 line, and thereafter the escape-region analysis is to be used. The initial condition E corresponds to the nominal GTO and the same tangential-thrust characteristics

[2] G. J. Whiffen, personal communication, Jet Propulsion Laboratory, Pasadena, California, November 2001.

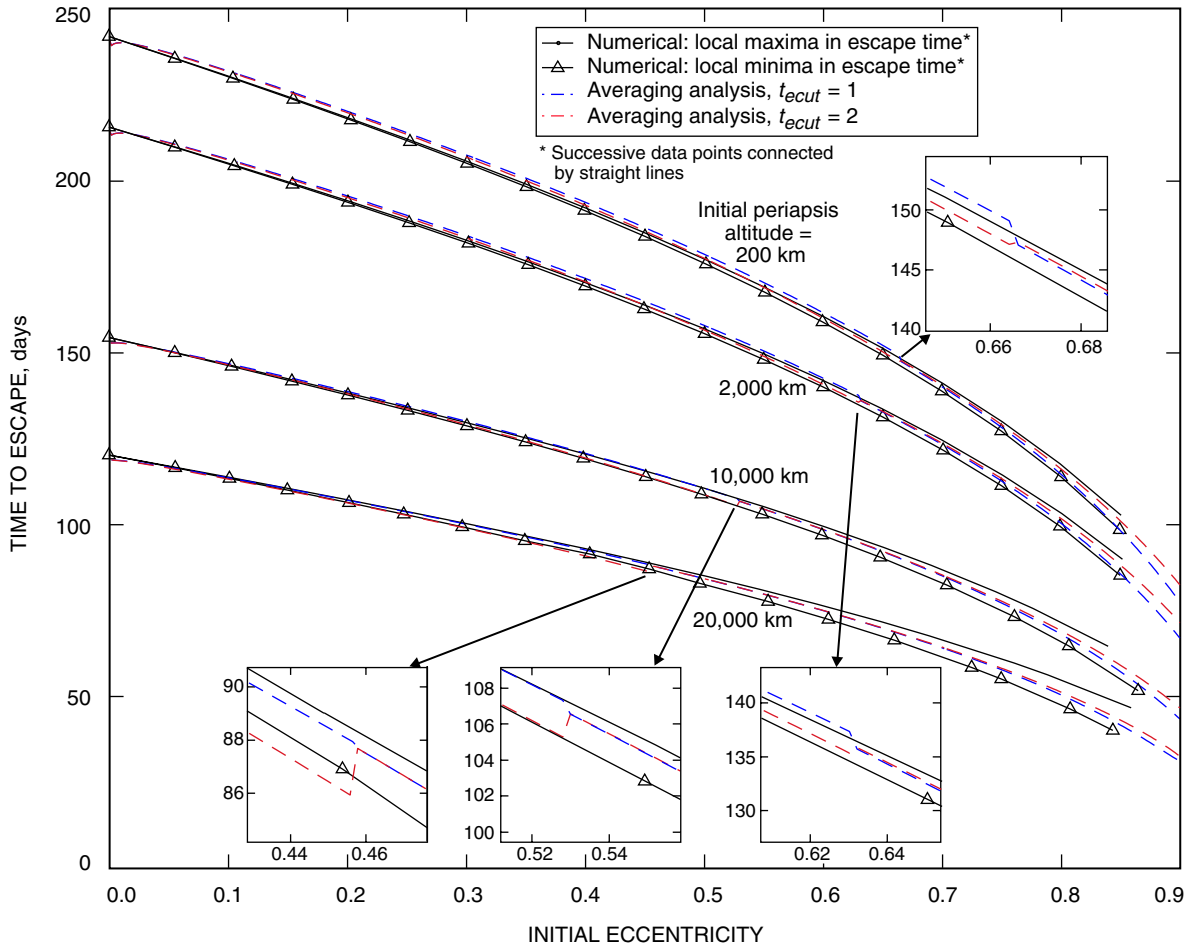

Fig. 8. Comparison of escape times computed by numerical integration and by the averaging analysis for a broad range of Earth orbits.

as before. The averaging contours for initial conditions E and F intersect the Q_2 line, whereupon the analysis must switch to the escape region. The initial conditions A and B are in the circular region, and so the traces approximately follow the circularization boundary from their outset.

Lastly, we examine the behavior of eccentricity and energy as functions of time for various escape spirals. We start with the two spirals of Fig. 3. The two traces of eccentricity versus time are reproduced in Fig. 10 together with curves from the averaging analysis. The initial conditions both lie in region E, very close to the nominal GTO (point E) in Fig. 9. As expected, due to the proximity of the initial conditions, the two curves based on averaging are almost indistinguishable from each other. The final, linear increase in eccentricity, starting at the S_2 point, occurs in the escape region of the ef-plot. A similar plot for the nominal GTO itself is shown in Fig. 11; energy versus time is shown in Fig. 12. High in the elliptic region of Fig. 9 are initial conditions F, which provide also the rightmost data point on the minimum-escape-time envelope for the 10,000-km periapsis grouping of Fig. 8. The corresponding averaged and integrated eccentricity and energy histories are shown in Figs. 13 and 14. Compared with the GTO analysis, these averaged histories show greater deviation from the integrated histories, most likely due to increased truncation errors and larger oscillations in the osculating eccentricity and energy on account of the increased thrust-to-semimajor-weight ratio.

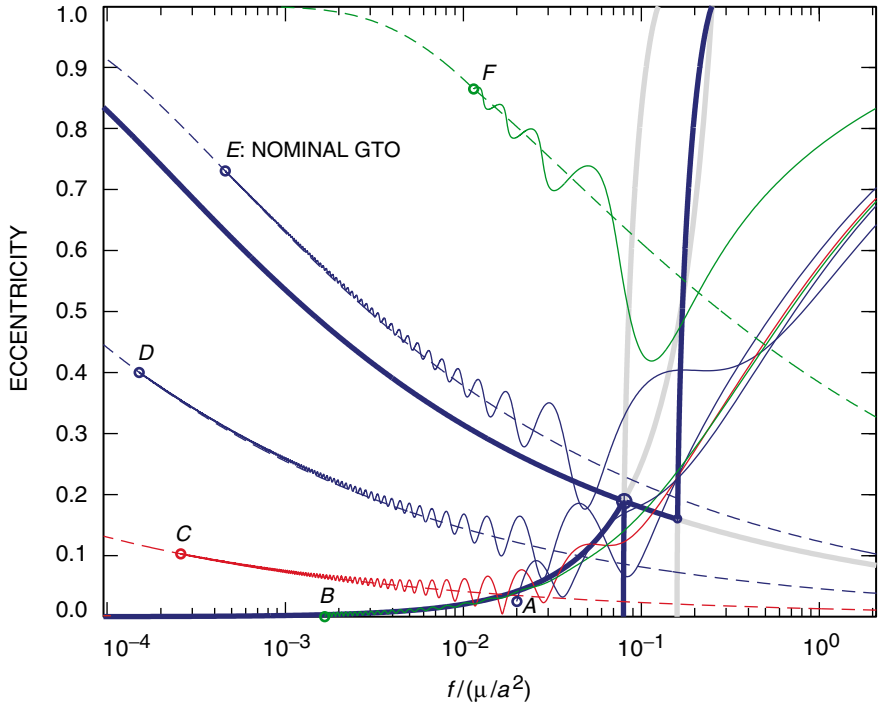

Fig. 9. Comparisons of spirals computed by numerical integration and by the averaging analysis for initial orbits lying in various regions of the ef-plot.

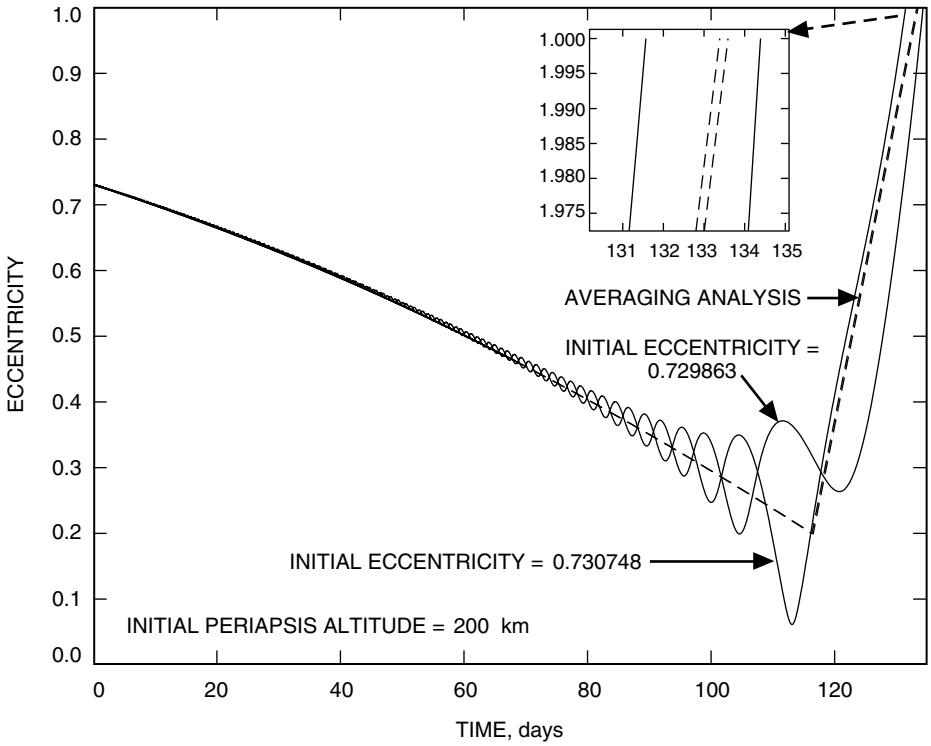

Fig. 10. Comparison of eccentricity as a function of time for the two near-GTO cases shown in Fig. 3, computed by numerical integration and by the averaging analysis.

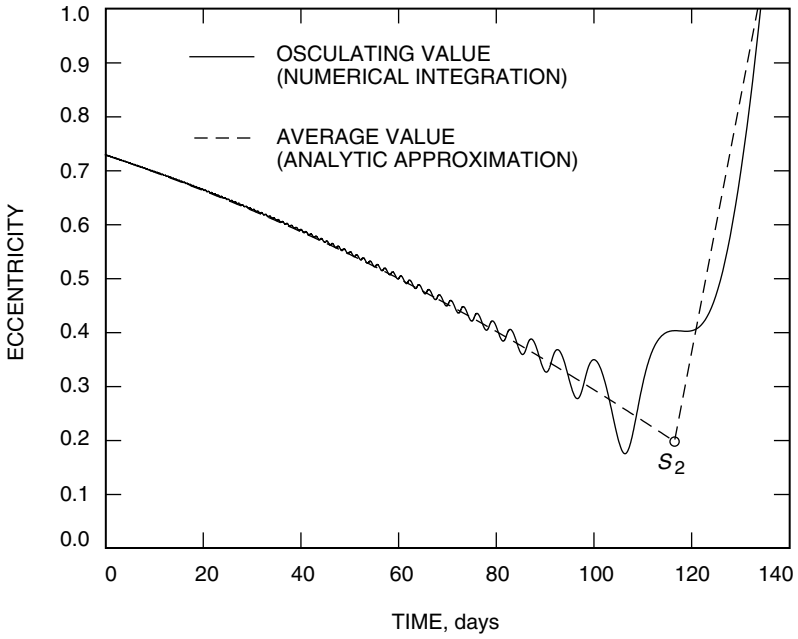

Fig. 11. Comparison of eccentricity as a function of time computed by numerical integration and by the averaging analysis for the nominal GTO initial orbit.

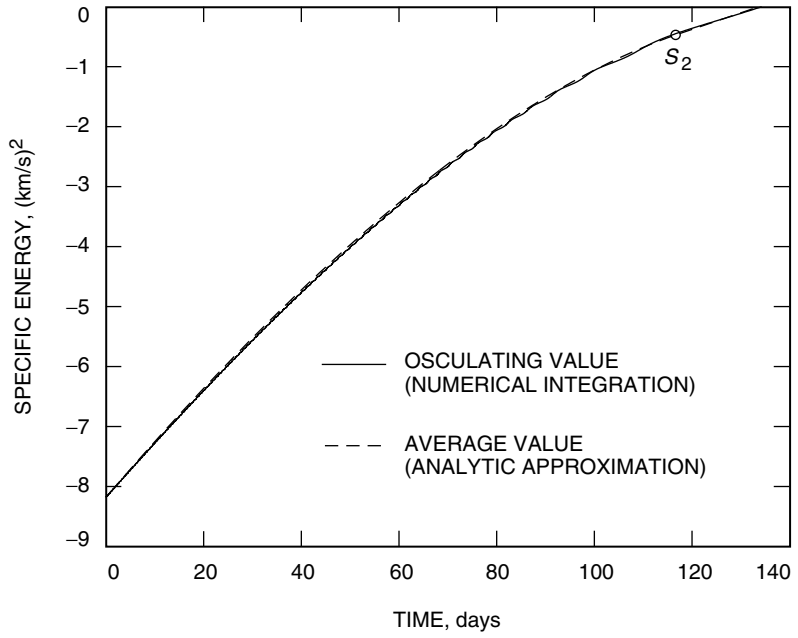

Fig. 12. Comparison of energy as a function of time computed by numerical integration and by the averaging analysis for the nominal GTO initial orbit.

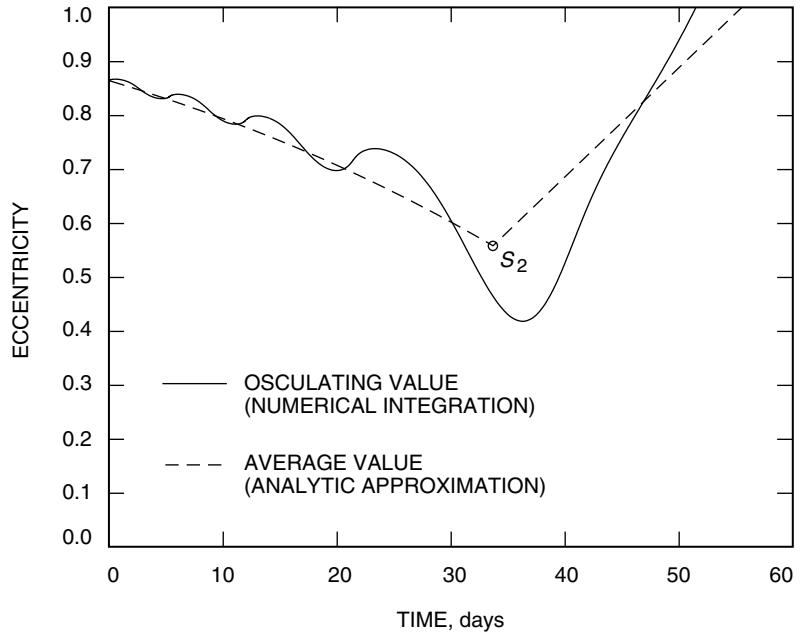

Fig. 13. Comparison of eccentricity as a function of time computed by numerical integration and by the averaging analysis for the point *F* initial orbit of Fig. 9 (periapsis altitude = 10,000 km, eccentricity = 0.86497).

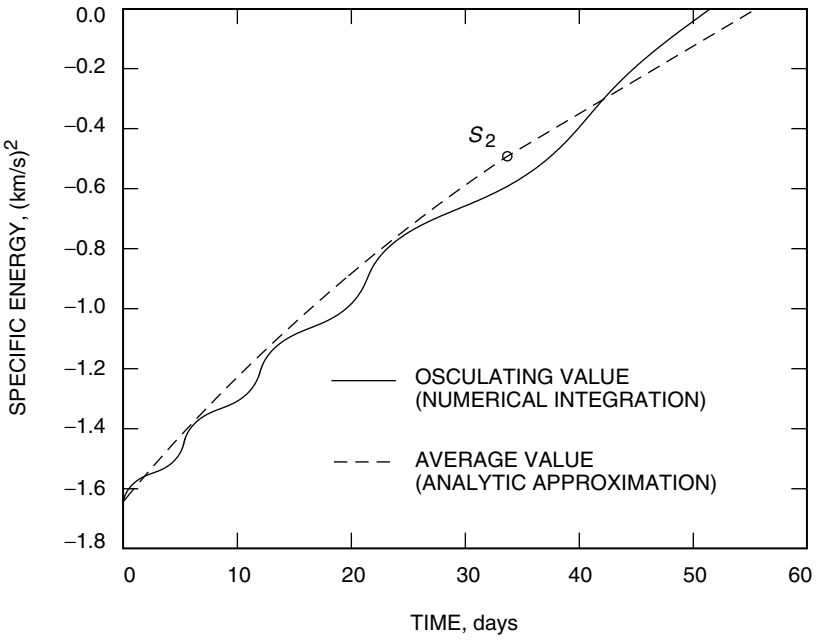

Fig. 14. Comparison of energy as a function of time computed by numerical integration and by the averaging analysis for the point *F* initial orbit of Fig. 9 (periapsis altitude = 10,000 km, eccentricity = 0.86497).

Points C and D of the semi-elliptic region in Fig. 9 correspond to data points on the lower envelopes for initial periapsis altitudes of 10,000 km and 2000 km, respectively, in Fig. 8. Eccentricity and energy histories are shown in Figs. 15 through 18. X_C marks the point where transition onto the circularization boundary occurs, and C_4 marks the point where the Q_4 line is crossed. In the case of energy, the difference between the averaging analysis and the numerical integration is not apparent at the scale of the plots up to about the X_4 point, where a slight divergence commences. For both C and D, the averaged eccentricity corresponds well with the integrated.

For the circular region points A and B of Fig. 9, eccentricity and energy versus time are shown in Figs. 19 through 22. In both cases, the small deviations of the averaged energy from the integrated slightly increase beyond about the C_4 point. Also, the deviation in case A is greater than in case B due to the larger initial thrust-to-semimajor-weight ratio (more than an order of magnitude greater than case B). For both A and B, the averaged eccentricity corresponds well with the integrated.

VI. Conclusions

Widely differing thrust histories can provide comparable, good performance in the problem of minimum-time, multi-revolution, constant-thrust escape or capture. Slight variations in the thrust profile, or, equivalently, the exact initial orbit, significantly affect the phasing of the final escape revolution. Phasing that provides an "escape from apoapsis" condition is seen to have lower escape times—essentially, enough thrust is available to circularize the orbit when the final apoapsis is reached, escaping shortly thereafter.

The need to select and integrate a precise thrust profile in order to compute the escape time is sidestepped by an averaging analysis that is developed for the full range of initial eccentricities (zero to almost one) and thrust-to-semimajor-weight ratios (that is, weight at a distance equal to the semimajor axis). In particular, analytic integrals are found for the averaged variational equations for energy and eccentricity. The averaging analysis also provides, with reasonable accuracy, relations between mean energy and mean eccentricity, as well as time as a function of these two quantities. Thus, the analysis can be used not only for escape and capture, but also for continuous-thrust, co-planar orbit transfers where the final argument of periapsis is free. Due to the analytic nature of the results, insights into the spiraling problem and key characteristics of spiraling trajectories can be found rapidly, without the need for numerical integration. Furthermore, the analytic relations obtained, as well as intermediate results leading up to them, could be of utility both in optimization based on averaging and in heuristic design of spirals involving coast arcs.

Acknowledgments

The author wishes to thank Jon A. Sims and Gregory J. Whiffen for their interest in, and encouragement of, the progress of this research. Thanks are also due to the latter for enthusiastically using his SDC software to compute a minimum-time escape-from-GTO spiral, which appears as a data point in this article.

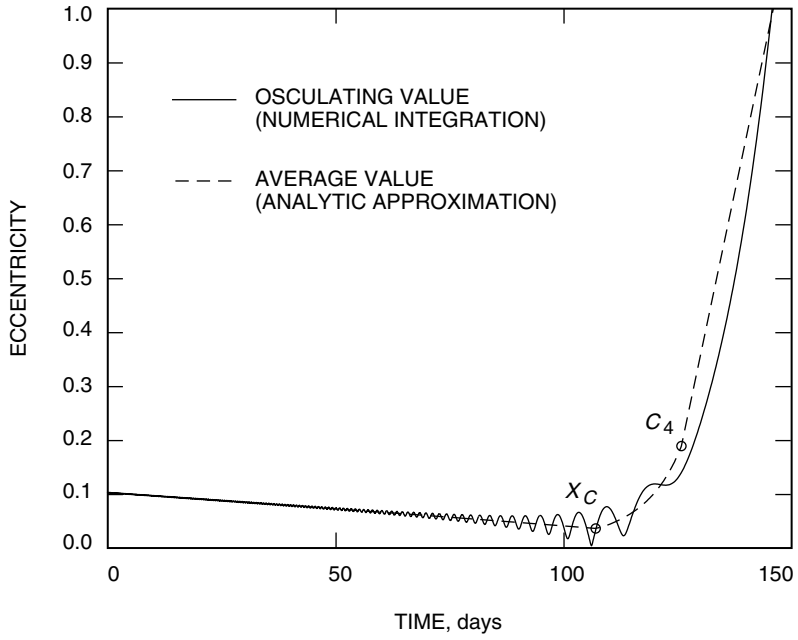

Fig. 15. Comparison of eccentricity as a function of time computed by numerical integration and by the averaging analysis for the point *C* initial orbit of Fig. 9 (periapsis altitude = 10,000 km, eccentricity = 0.10301).

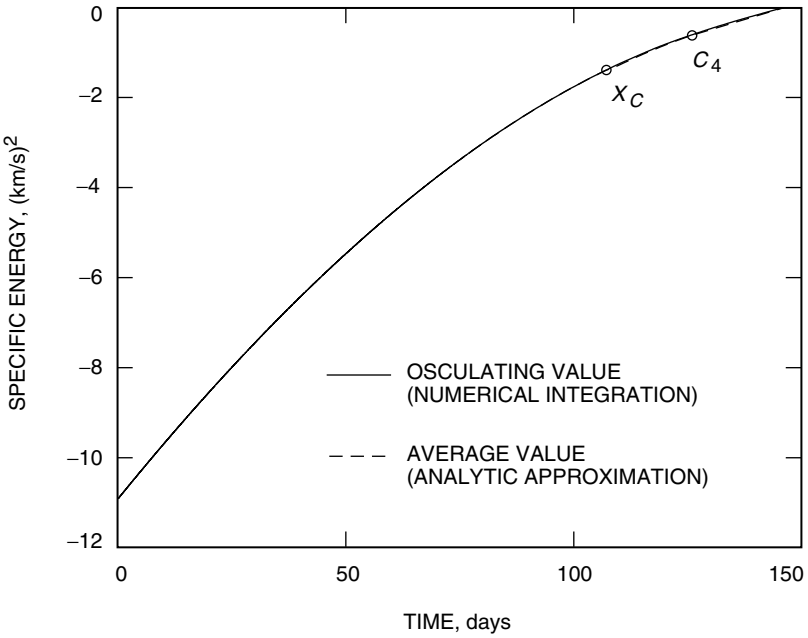

Fig. 16. Comparison of energy as a function of time computed by numerical integration and by the averaging analysis for the point *C* initial orbit of Fig. 9 (periapsis altitude = 10,000 km, eccentricity = 0.10301).

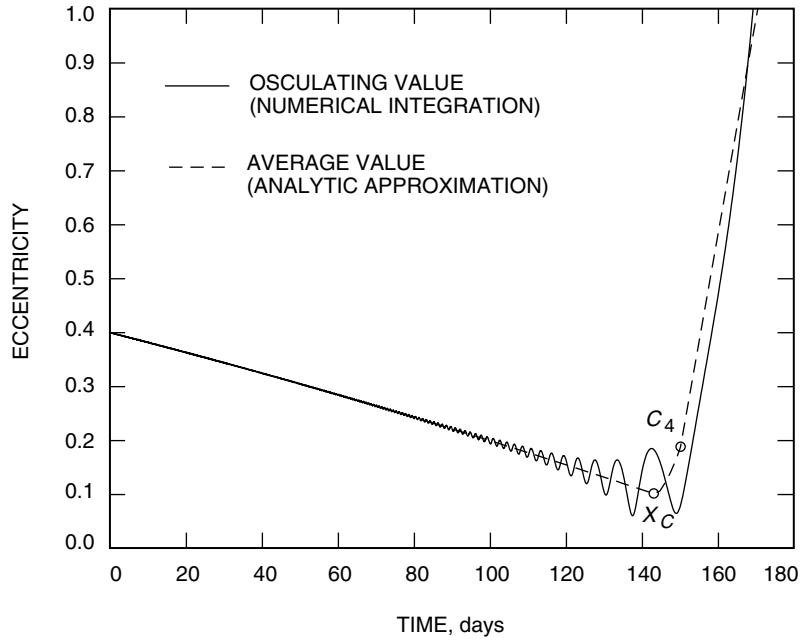

Fig. 17. Comparison of eccentricity as a function of time computed by numerical integration and by the averaging analysis for the point *D* initial orbit of Fig. 9 (periapsis altitude = 2,000 km, eccentricity = 0.40034).

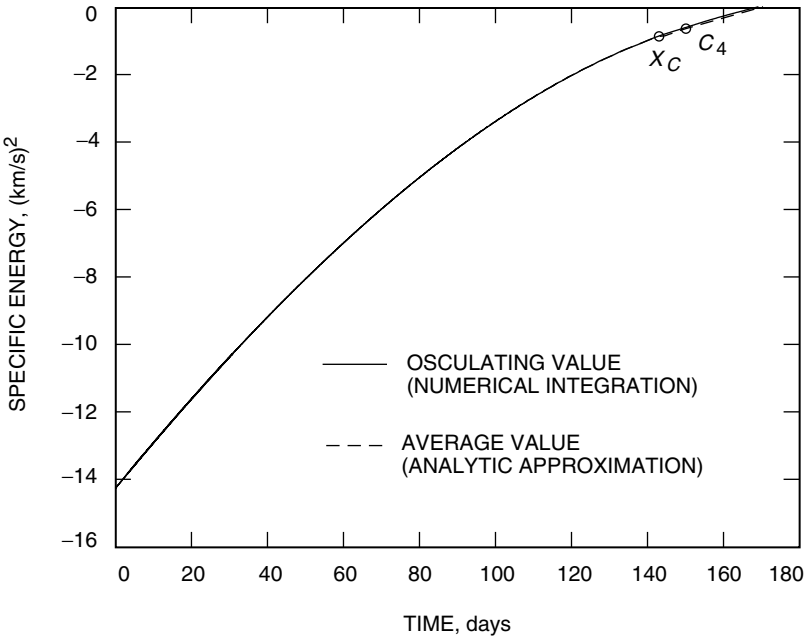

Fig. 18. Comparison of energy as a function of time computed by numerical integration and by the averaging analysis for the point *D* initial orbit of Fig. 9 (periapsis altitude = 2,000 km, eccentricity = 0.40034).

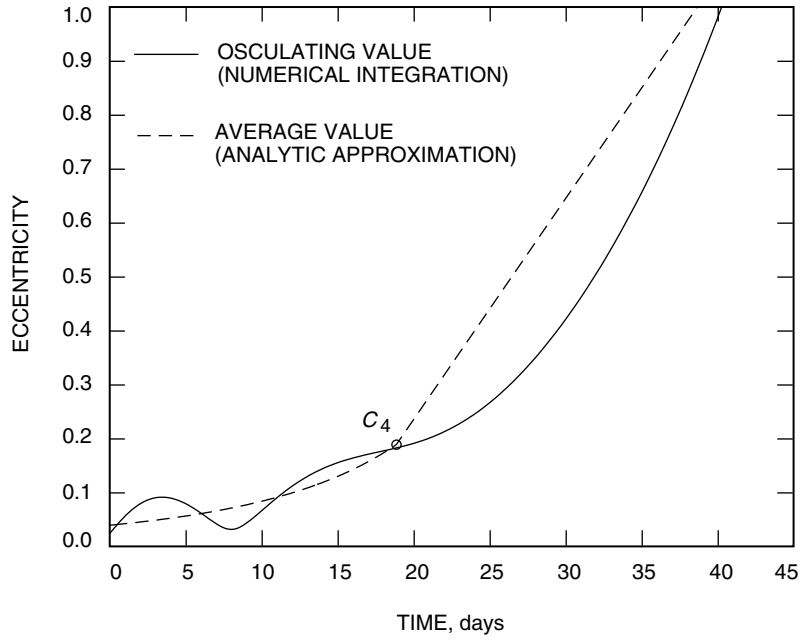

Fig. 19. Comparison of eccentricity as a function of time computed by numerical integration and by the averaging analysis for the point *A* initial orbit of Fig. 9 (periapsis altitude = 150,000 km, eccentricity = 0.025).

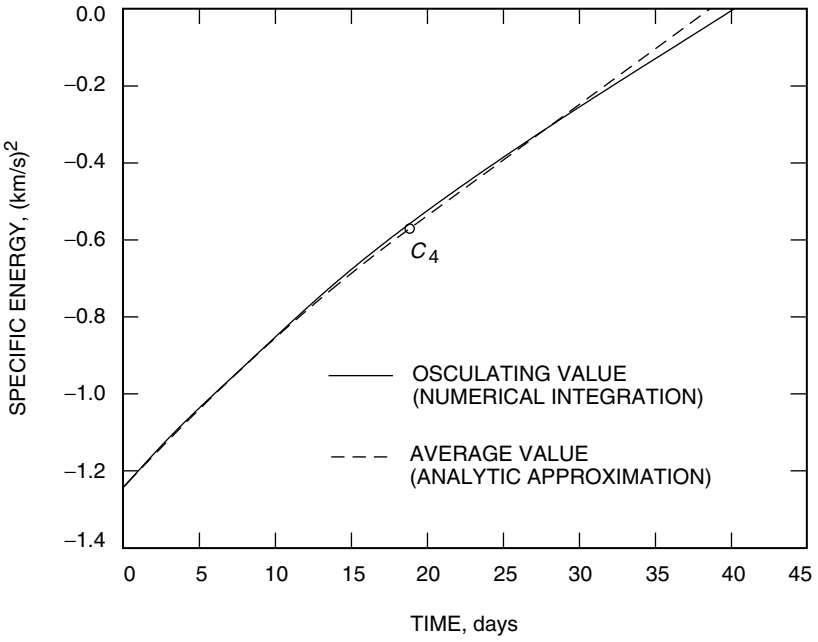

Fig. 20. Comparison of energy as a function of time computed by numerical integration and by the averaging analysis for the point *A* initial orbit of Fig. 9 (periapsis altitude = 150,000 km, eccentricity = 0.025).

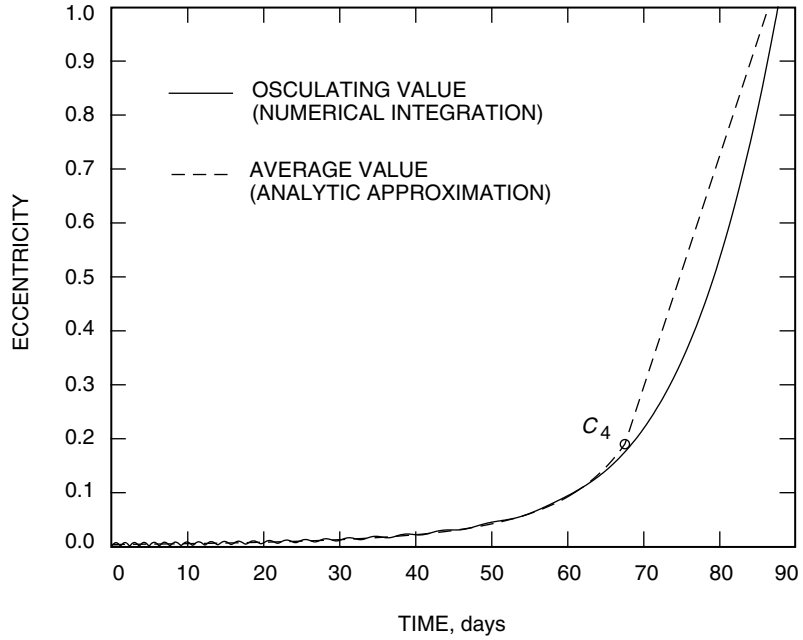

Fig. 21. Comparison of eccentricity as a function of time computed by numerical integration and by the averaging analysis for the point *B* initial orbit of Fig. 9 (circular orbit altitude = 40,000 km).

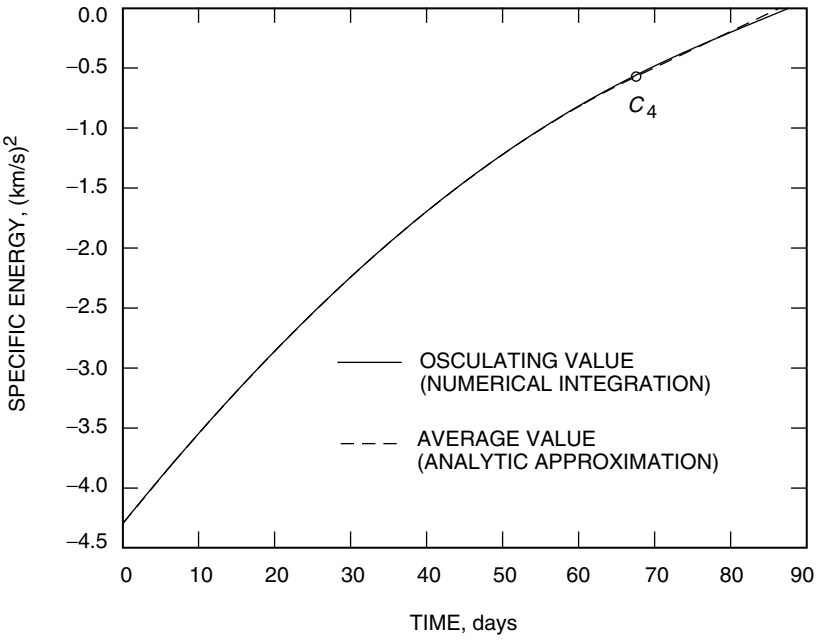

Fig. 22. Comparison of energy as a function of time computed by numerical integration and by the averaging analysis for the point *B* initial orbit of Fig. 9 (circular orbit altitude = 40,000 km).

References

[1] D. F. Lawden, "Optimal Programming of Rocket Thrust Direction," *Astronautica Acta,* vol. 1, pp. 41–56, 1955.

[2] D. F. Lawden, "Optimal Escape from a Circular Orbit," *Astronautica Acta,* vol. 4, pp. 218–233, 1958.

[3] H. S. Tsien, "Take-off from Satellite Orbit," *J. American Rocket Society,* vol. 23, pp. 233–236, July–August 1953.

[4] D. J. Benney, "Escape from a Circular Orbit Using Tangential Thrust," *Jet Propulsion,* vol. 28, pp. 167–169, March 1958.

[5] G. F. Forbes, "The Trajectory of a Powered Rocket in Space," *Journal of the British Interplanetary Society,* vol. 9, no. 2, pp. 75–79, 1950 (abridgement of Master's Thesis submitted to the Massachusetts Institute of Technology).

[6] T. C. Tsu, "Interplanetary Travel by Solar Sail," *J. American Rocket Society,* vol. 29, pp. 422–427, 1959.

[7] F. M. Perkins, "Flight Mechanics of Low-Thrust Spacecraft," *Journal of the Aero/Space Sciences,* vol. 26, pp. 291–297, May 1959.

[8] G. Pinkham, "Reference Solution for Low Thrust Trajectories," *J. American Rocket Society,* vol. 32, no. 5, pp. 775–776, May 1962.

[9] W. G. Melbourne, *Interplanetary Trajectories and Payload Capabilities of Advanced Propulsion Vehicles,* NASA Technical Report 32-68, Jet Propulsion Laboratory, Pasadena, California, March 31, 1961.

[10] W. G. Melbourne and C. G. Sauer, Jr., "Performance Computations with Pieced Solutions of Planetocentric and Heliocentric Trajectories for Low-Thrust Missions," *Space Programs Summary 37-36,* vol. IV, Jet Propulsion Laboratory, Pasadena, California, pp. 14–19, December 31, 1965.

[11] H. M. Stark and P. D. Arthur, "Simple Approximate Solutions for Tangential, Low-Thrust Trajectories," *Journal of the Aerospace Sciences,* pp. 897–898, November 1961.

[12] C.-H. Zee, "Low-Thrust Oscillatory Spiral Trajectory," *Astronautica Acta,* vol. 9, pp. 201–207, 1963.

[13] C.-H. Zee, "Low Constant Tangential Thrust Spiral Trajectories," *AIAA Journal,* vol. 1, no. 7, pp. 1581–1583, July 1963.

[14] C.-H. Zee, "Spatial Powered Flight Trajectories of Space Vehicles Under Oriented Constant Thrust," *Astronautica Acta,* vol. 9, pp. 107–114, 1963.

[15] C.-H. Zee, "Powered Flight Trajectories of Rockets under Oriented Constant Thrust," *AIAA Journal,* vol. 1, no. 3, pp. 602–606, March 1963.

[16] C.-H. Zee, "Powered Flight Trajectories of Rockets under Constant Tangential Thrust," *Journal of the Astronautical Sciences,* vol. 12, no. 1, pp. 1–6, Spring 1965.

[17] D. P. Johnson and L. W. Stumpf, "Perturbation Solutions for Low-Thrust Rocket Trajectories," *AIAA Journal,* vol. 3, no. 10, pp. 1934–1936, October 1965.

[18] Y.-Y. Shi and M. C. Eckstein, "Ascent or Descent from Satellite Orbit by Low Thrust," *AIAA Journal,* vol. 4, no. 12, pp. 2203–2209, December 1966.

[19] Y.-Y. Shi and M. C. Eckstein, "An Approximate Solution for Ascending Low-Thrust Trajectories without Singularity," *AIAA Journal,* vol. 5, no. 1, pp. 170–172, January 1967.

[20] A. H. Nayfeh, "Take-Off from a Circular Orbit by a Small Thrust," AIAA Paper 65-688, September 1965; also AIAA *Progress in Astronautics and Aeronautics: Methods in Astrodynamics and Celestial Mechanics,* vol. 17, R. L. Duncombe and V. G. Szebehely, eds., New York: Academic Press Inc., pp. 139–157, 1966.

[21] N. Markopoulos, "Non-Keplerian Manifestations of the Keplerian Trajectory Equation and a Theory of Orbital Motion Under Continuous Thrust," AAS/AIAA Space Flight Mechanics Meeting, AAS Paper 95-217, Albuquerque, New Mexico, February 1995.

[22] J. E. Prussing and V. Coverstone-Carroll, "Constant Radial Thrust Acceleration Redux," *J. Guidance, Control, and Dynamics,* vol. 21, no. 3, pp. 516–518, May–June 1998.

[23] J. A. Kechichian, "Orbit Raising with Low-Thrust Tangential Acceleration in Presence of Earth Shadow," *Journal of Spacecraft and Rockets,* vol. 35, no. 4, pp. 516–525, July–August 1998.

[24] A. E. Petropoulos, J. M. Longuski, and N. X. Vinh, "Shape-Based Analytic Representations of Low-Thrust Trajectories for Gravity-Assist Applications," AAS/AIAA Astrodynamics Specialist Conference, AAS Paper 99-337, Girdwood, Alaska, August 1999.

[25] A. A. Sukhanov and A. F. B. de A. Prado, "Constant Tangential Low-Thrust Trajectories near an Oblate Planet," *Journal of Guidance, Control, and Dynamics,* vol. 24, no. 4, pp. 723–731, July–August 2001.

[26] C. Marchal, J.-P. Marec, and C. B. Winn, "Synthesis of the Analytical Results on Optimal Transfers between Keplerian Orbits," Library Translation no. 1281, Royal Aircraft Establishment, Farnborough Hants, United Kingdom, March 1968; translation of ONERA T. P. 515, 1967.

[27] C. Marchal, "Synthése des Résultats Analytique sur les Transferts Optimaux entre Orbites Képlériennes," *Advanced Problems and Methods for Space Flight Optimization,* Proceedings of Colloquium at the University of Liège, Belgium, B. Fraeijs de Veubeke, ed., Oxford: Pergamon Press, pp. 91–156, 1969.

[28] G. L. Grodzovskii, Y. N. Ivanov, and V. V. Tokarev, *Mechanics of Low-Thrust Spaceflight,* translated from the Russian, A. Baruch, transl., Y. M. Timant, ed., NASA TTF-507, TT 68-50301, Israel Program for Scientific Translation, Jerusalem, 1969.

[29] D. F. Lawden, "Optimal Intermediate-Thrust Arcs in a Gravitational Field," *Astronautica Acta,* vol. 8, pp. 106–123, 1962.

[30] D. F. Lawden, *Optimal Trajectories for Space Navigation,* London: Butterworths, 1963.

[31] R. H. Bishop and D. M. Azimov, "New Analytic Solutions to the Fuel-Optimal Orbital Transfer Problem Using Low-Thrust Exhaust-Modulated Propulsion," AAS/AIAA Space Flight Mechanics Meeting, AAS Paper 00-131, Clearwater, Florida, January 2000.

[32] J. Kevorkian and J. D. Cole, *Multiple Scale and Singular Perturbation Methods,* New York: Springer Verlag, 1996.

[33] T. N. Edelbaum, "Optimum Low-Thrust Transfer between Circular and Elliptic Orbits," *Proceedings of the Fourth U.S. National Congress on Applied Mechanics,* American Society of Mechanical Engineers, New York, pp. 137–141, 1962.

[34] T. N. Edelbaum, "Optimum Power-Limited Orbit Transfer in Strong Gravity Fields," *AIAA Journal,* vol. 3, no. 5, pp. 921–925, May 1965.

[35] J.-P. Marec and N. X. Vinh, "Optimal Low-Thrust, Limited Power Transfers between Arbitrary Elliptical Orbits," *Acta Astronautica,* vol. 4, pp. 511–540, 1977.

[36] L. L. Sackett, H. L. Malchow, and T. N. Edelbaum, *Solar Electric Geocentric Transfer with Attitude Constraints: Analysis,* NASA CR-134927, The Charles Stark Draper Laboratory, Inc., Cambridge, Massachusetts, August 1975.

[37] S. Geffroy and R. Epenoy, "Optimal Low-Thrust Transfers with Constraints—Generalization of Averaging Techniques," *Astronautica Acta,* vol. 41, no. 3, pp. 133–149, 1997.

[38] C. A. Kluever and S. R. Oleson, "A Direct Approach for Computing Near-Optimal Low-Thrust Transfers," AAS/AIAA Astrodynamics Specialist Conference, AAS Paper 97-717, Sun Valley, Idaho, August 4–7, 1997.

[39] J. T. Betts, "Very Low-Thrust Trajectory Optimization Using a Direct SQP Method," *Journal of Computational and Applied Mathematics,* no. 120, pp. 27–40, 2000.

[40] J. A. Kechichian, "Minimum-Time Constant Acceleration Orbit Transfer with First-Order Oblateness Effect," *Journal of Guidance, Control, and Dynamics,* vol. 23, no. 4, pp. 595–603, July–August 2000.

[41] J. D. Thorne and C. D. Hall, "Minimum-Time Continuous-Thrust Orbit Transfers," *Journal of the Astronautical Sciences,* vol. 45, no. 4, pp. 411–432, October–December 1997.

[42] Y. Hui and W. Hongxin, "Initial Adjoint Variable Guess Technique and its Application in Optimal Orbital Transfer," AIAA/AAS Astrodynamics Specialist Conference, AIAA Paper 98-4551, Boston, Massachusetts, August 10–12, 1998.

[43] G. J. Whiffen and J. A. Sims, "Application of a Novel Optimal Control Algorithm to Low-Thrust Trajectory Optimization," AAS/AIAA Space Flight Mechanics Meeting, AAS Paper 01-209, Santa Barbara, California, February 11–15, 2001.

[44] G. J. Whiffen and J. A. Sims, "Application of the SDC Optimal Control Algorithm to Low-Thrust Escape and Capture Trajectory Optimization," AAS/AIAA Space Flight Mechanics Meeting, AAS Paper 02-208, San Antonio, Texas, January 27–30, 2002.

[45] A. E. Petropoulos, G. J. Whiffen, and J. A. Sims, "Simple Control Laws for Continuous-Thrust Escape or Capture and Their Use in Optimisation," AIAA/AAS Astrodynamics Specialist Conference, AIAA Paper 2002-4900, Monterey, California, August 5–8, 2002.

[46] C. A. Kluever, "Simple Guidance Scheme for Low-Thrust Orbit Transfers," *J. Guidance, Control, and Dynamics,* vol. 21, no. 6, pp. 1015–1017, November 1998.

[47] L. P. Gefert and K. J. Hack, "Low-Thrust Control Law Development for Transfer from Low Earth Orbits to High Energy Elliptical Parking Orbits," AAS/AIAA Astrodynamics Specialist Conference, AAS Paper 99-410, Girdwood, Alaska, August 1999.

[48] R. H. Battin, *An Introduction to the Mathematics and Methods of Astrodynamics,* 1st. ed., 4th. printing, New York: AIAA, 1987.

[49] I. S. Gradshteyn and I. M. Ryzhik, *Table of Integrals, Series, and Products,* 5th. ed., Boston: Academic Press, Inc., 1994.